XI International Conference on Computational Plasticity. Fundamentals and Applications
COMPLAS XI
E. Oñate, D.R.J. Owen, D. Peric and B. Suárez (Eds)

2D ADAPTIVE FEM SIMULATION OF FAILURES IN HIGH-SPEED IMPACTS

M.Issa[1], K.Saanouni[1], C.Labergère[1], A.Rassineux[2]

[1]ICD/LASMIS, UMR CNRS 6279, Université de Technologie de Troyes, BP 2060, 10010 Troyes Cedex, France
mazen.issa@utt.fr, saanouni@utt.fr, labergere@utt.fr
[2]Laboratoire Roberval de Mécanique, UMR CNRS 6259, Université de technologie de Compiègne, BP 20529, 60205 Compiègne Cedex, France.
alain.rassineux@utc.fr

Key words: thermo-elasto-visco-plasticity, finite strains, ductile damage, mixed hardening, full coupling, 2D adaptive mesh, error estimates, high velocity impact, FEM.

Abstract. The simulation of high-speed impacts needs the use of advanced constitutive equations required for the accurate prediction of the different thermomechanical fields and their mutual interactions (temperature, large strains, hardening, damage, friction …). Since these fields localize inside intense shear bands (ISB), ductile micro-cracks initiate inside these ISB leading to the initiation of macroscopic crack and its fast propagation until the final fracture occurs. Accordingly, these advanced constitutive equations should take into account not only the strong thermomechanical coupling but also the ductile damage and its strong effect (coupling) on the other thermomechanical fields. In this work a complete set of advanced and fully coupled thermo-elasto-viscoplastic-damage constitutive equations accounting for mixed nonlinear isotropic and kinematic hardening fully coupled with the ductile isotropic damage and the thermal softening for time dependent finite plasticity is presented. Related numerical aspects in the framework of a fully adaptive 2D finite element strategy are developed and briefly discussed. This adaptive procedure is applied to the simulation of simple high velocity impact of thick sheets with dynamic ductile fracture occurrence. Attention is paid to the localization of the main thermomechanical fields inside the ISB as well as to the macroscopic cracks initiation and growth under high velocity impact.

1 INTRODUCTION

High speed impact is mostly used to investigate the material behaviour under dynamic (high velocity) loading conditions where the strain rates can locally reach 10^8 s^{-1}. For strain rates in between 10 s^{-1} and 10^4 s^{-1} the impact tests can be investigated using the Hopkinson bar facilities, and between 10^4 s^{-1} and 10^8 s^{-1} the so called Taylor impact experimental

procedure should be used where the data analysis is more complex to investigate. Note that Taylor [1] was the first who developed analytical method to assess the dynamic yield stress at different strain rates for various materials. Other research works have investigated the high speed impacts on several metals like steel, aluminium and cooper [2-4]**.** More information about recent high speed experimental studies can be found in [5-8] where many of high speed impact works are reviewed.

The numerical simulations of high speed impact should take into account the highly severe thermomechanical conditions i.e.: high temperature which can exceeds the melting temperature, high strain rates reaching the 10^8 s^{-1}, large viscoplastic strains and complex contact and friction conditions. These fully coupled phenomena and their interactions should be accounted for in any constitutive equations used for their numerical simulation. Recently, different material behaviour models are used to simulate the high speed machining processes. These constitutive equations often propose a weak thermal coupling and isotropic viscoplastic flow with isotropic hardening of Norton-Hoff or Johnson-Cook types. In these models, many numerical formulations have been used like updated Lagrangian formulation ([10], [12-22], [25]), Eulerian formulation [9] or arbitrary Lagrangian Eulerian (ALE) formulations ([11-12]) have been used. Other works use specific meshless based numerical approaches to avoid the mesh adaptivity ([20]-[22]). In this work, an adaptive 2D FE-based numerical methodology using advanced constitutive equations which account for the ductile damage and its effect on the other thermomechanical fields at finite strain is presented. The coupling between thermal aspects, thermo-elasto-viscoplasticity and ductile damage including the mixed isotropic and kinematic non-linear hardening are included in this model previously developed by Saanouni et al. ([23]-[28]). Using the Vumat subroutine, the developed model is implemented into ABAQUS/EXPLICIT. Using this fully coupled methodology, the typical example of dynamic impact is investigated and attention is paid to the prediction of the thermomechanical fields' localization inside ISB where macroscopic cracks initiate and evolve with high velocity until the final fracture occurs.

2 THERMO-ELASTO-VISCOPLASTIC DAMAGE MODEL

In the framework of the thermodynamics of irreversible processes with state variables, and assuming small elastic and large viscoplastic strains, fully coupled thermo-elasto-visco-plastic-damage constitutive equations accounting for the micro-cracks closure are developed. Two external state variables are used: ($\underline{\varepsilon} = \int_t \underline{D} dt$, $\underline{\sigma}$) for mechanical aspects and (T, s) for thermal phenomena. For 'internal' state variables and their conjugate forces we have: ($\underline{\varepsilon}^e$, $\underline{\sigma}$) for small elastic strain tensor and the Cauchy stress tensor; ($\vec{q}, \vec{g} = \overrightarrow{grad(T)}$) for heat flux vector and its conjugate force; ($\underline{\alpha}$, $\underline{X}$) for the kinematic hardening (i.e. translation of the yield surface center); (r, R) for the isotropic hardening (i.e. variation of the yielding surface size) and (D,Y) for isotropic damage and its conjugate force.

Following this approach, a complete set of fully coupled constitutive equations is deduced in which the state relations (1) to (4) and the evolution equations (5) to (8) are summarized as following:

- **State relations:**

$$\underline{\sigma} = <\underline{\sigma}>_+ + <\underline{\sigma}>_- \text{ where } \begin{cases} <\underline{\sigma}>_+ = & \frac{\nu E(1-D)}{(1+\nu)(1-2\nu)} <\underline{\varepsilon}^e : \underline{1}>_+ <\underline{1}>_+ + \frac{E(1-D)}{(1+\nu)} <\underline{\varepsilon}^e>_+ \\ & -\frac{E}{(1-2\nu)} \xi\sqrt{1-D}(T-T_0) <\underline{1}>_+^{\varepsilon} \\ <\underline{\sigma}>_- = & \frac{\nu E(1-hD)}{(1+\nu)(1-2\nu)} <\underline{\varepsilon}^e : \underline{1}>_- <\underline{1}>_- + \frac{E(1-hD)}{(1+\nu)} <\underline{\varepsilon}^e>_- \\ & -\frac{E}{(1-2\nu)} \xi\sqrt{1-hD}(T-T_0) <\underline{1}>_-^{\varepsilon} \end{cases} \quad (1)$$

$$s = \frac{1}{\rho}\frac{E}{(1-2\nu)}\xi\sqrt{1-D} <\underline{\varepsilon}^e : \underline{1}>_+ + \frac{1}{\rho}\frac{E}{(1-2\nu)}\xi\sqrt{1-hD} <\underline{\varepsilon}^e : \underline{1}>_- + C_v\frac{(T-T_0)}{T_0} \quad (2)$$

$$\underline{X} = \frac{2C(1-D)}{3}\underline{\alpha} \quad \text{(a)} \qquad R = (1-D^m)Qr \quad \text{(b)} \quad (3)$$

$$\begin{cases} Y = <Y_{el}>_+ + <Y_{el}>_- + Y_{in} \\ <Y_{el}>_+ = \frac{\nu E}{2(1+\nu)(1-2\nu)} <\underline{\varepsilon}^e : \underline{1}>_+^2 + \frac{E}{2(1+\nu)} <\underline{\varepsilon}^e>_+ : <\underline{\varepsilon}^e>_+ - \frac{E}{2\sqrt{1-D}(1-2\nu)}\xi(T-T_0) <\underline{\varepsilon}^e : \underline{1}>_+ \\ <Y_{el}>_- = h\left[\frac{h\nu E}{2(1+\nu)(1-2\nu)} <\underline{\varepsilon}^e : \underline{1}>_-^2 + \frac{hE}{2(1+\nu)} <\underline{\varepsilon}^e>_- : <\underline{\varepsilon}^e>_- - \frac{hE}{2\sqrt{1-hD}(1-2\nu)}\xi(T-T_0) <\underline{\varepsilon}^e : \underline{1}>_-\right] \\ Y_{in} = \frac{1}{3}C\underline{\alpha} : \underline{\alpha} + mD^{(m-1)}\frac{1}{2}Qr^2 \end{cases} \quad (4)$$

where: (E, ν): Young modulus and Poisson coefficient, T: temperature, T_0: reference temperature, ξ: thermal expansion coefficient, C: kinematic hardening modulus, Q: isotropic hardening modulus, C_v: specific heat coefficient, ρ: material density, Y_{el}: the elastic part of the damage energy release rate and Y_{in}: its inelastic counter part, m a material parameter and $0 < h < 1$ is the micro-cracks closure parameter.

- **Evolution equations:**

$$\underline{D}^{vp} = \dot{\lambda}_{vp}\underline{n} \quad \text{(a)} \qquad \underline{n} = \frac{3}{2\sqrt{1-D}}\frac{\left(\underline{\sigma}^{dev} - \underline{X}\right)}{\left\|\underline{\sigma} - \underline{X}\right\|_M} \quad \text{(b)} \quad (5)$$

$$\dot{\underline{\alpha}}^{vp} = \dot{\lambda}_{vp}(\underline{n} - a\underline{\alpha}) \quad \text{(a)} \qquad \dot{r} = \dot{\lambda}_{vp}\left(\frac{1}{(1-D^m)} - br\right) \quad \text{(b)} \quad (6)$$

$$\dot{D} = \frac{\dot{\lambda}_{vp}}{(1-D)^{\beta}}\left[\frac{\langle Y - Y_0\rangle}{S}\right]^s \quad \text{(a)} \qquad \vec{q} = -k\overrightarrow{gradT} \quad \text{(b)} \quad (7)$$

$$f_{vp}(\underline{\sigma}, \underline{X}, R, \dot{p}; D) = f(\underline{\sigma}, \underline{X}, R; D) - K_2 Arc\sinh\left(\frac{\sqrt{1-D}\,\dot{p}}{K_1}\right) \le 0 \quad (8)$$

$$f(\underline{\sigma},\underline{X},R;D)=\frac{\left\|\underline{\sigma}-\underline{X}\right\|_M}{\sqrt{1-D}}-\frac{R}{\sqrt{1-D^m}}-\sigma_y \tag{9}$$

In these equations a and b are the material parameters governing the non-linearity of kinematic and isotropic hardening respectively. S, s, Y_0 and β are the ductile damage parameters.

$\dot{\lambda}_{vp}$ is the viscoplastic multiplier defined by $\dot{\lambda}_{vp}=K_1 Sinh\langle f/K_2\rangle$ which in fact is taken as the main unknown to be determined numerically at each integration point. K_1 and K_2 are the viscous parameters and f_{vp} is the viscoplastic yield function defined in Eq.8. The deviatoric tensor $\underline{n}$ in Eq.5b defines the outward normal to this yield function. The equivalent viscoplastic deformation rate is defined by $\dot{p}=\sqrt{(2/3)\underline{\dot{\varepsilon}}^{vp}:\underline{\dot{\varepsilon}}^{vp}}=\dot{\lambda}_{vp}/\sqrt{1-D}$ and the von Mises equivalent stress is given by: $\left\|\underline{\sigma}-\underline{X}\right\|_M=\sqrt{(3/2)(\underline{\sigma}-\underline{X})^{dev}:(\underline{\sigma}-\underline{X})^{dev}}$.

Combining Eq.7b (where k is the thermal conductivity) with the first law of thermodynamics leads to the generalized heat equation governing the temperature evolution under the form:

$$\rho C_v\dot{T}-k\Delta T=\underline{\sigma}:\underline{D}^{vp}-\underline{X}:\underline{\dot{\alpha}}-R\dot{r}+Y\dot{D}+\pi+T\left[\frac{\partial\underline{\sigma}}{\partial T}:\underline{\dot{\varepsilon}}^{e}-\frac{\partial Y}{\partial T}\dot{D}+\frac{\partial\underline{X}}{\partial T}:\underline{\dot{\alpha}}+\frac{\partial R}{\partial T}\dot{r}\right] \tag{10}$$

Note that, in this study, only the following material properties: E, C, Q, S, K_1 and σ_y, are taken as temperature dependent according to the simple relation of the form:

$$p=p_0\left[1-\left((T-T_0)/T_f-T_0\right)^{\chi}\right] \tag{11}$$

where $P\in\{E,C,Q,S,K_1,\sigma_y\}$ is the value of any of these parameters at the temperature T, P_0 its value at the reference temperature T_0, T_f is the melting temperature of the material and χ is a temperature independent material parameter.

The numerical aspects of the presented model and their implementation in ABAQUS/EXPLICIT is detailed in ([24-27]). A dynamic explicit scheme is used for the resolution of the global equilibrium and temperature equations, for the numerical integration of the fully coupled constitutive equations at each Gauss point of each element, the stress tensor as well as the overall state variables at each time increment, is calculated by iterative implicit algorithm using the elastic prediction and viscoplastic correction procedure with radial return mapping algorithm applied to a reduced number of differential equations.

A 2D mesh generator named DIAMESH2D is used for the 2D adaptive analysis following the procedure described in [26]. Based on appropriate error indicators with 2D linear and quadratic Quadrangular and Triangular elements, this procedure adapts the mesh size and the loading sequence with respect to the local curvature of the contact surfaces and to the distribution of the plastic and damage dissipations.

3 Application to high speed shear impact

This example concerns a typical dynamic (high speed) impact test performed using AISI4340 steel cylindrical sample composed from a hollow cylinder connected with a solid one, as schematically shown in Fig.1. Basing on the force displacement curves given in [28] for the AISI4340 stainless steel, the material parameters of the sample are determined using a classical inverse approach. The obtained values are: E=205000 MPa, ν=0.3, Cv=457 J/kg°C, ξ=1.37 10^{-5} °C^{-1} for the thermo elasticity. σ_y=792 MPa, Q=320 MPa, C= 5000 MPa, b=0.6, a=20, K_1=48.9, K_2=79.38 MPa for the viscoplastisity and S= 20, s=2, β=1, Y_0=7 for the damage evolution equations. All these parameters are identified at the reference temperature T_0= 20°C and their evolutions with respect to the temperature are governed by Eq. (11) in which the parameter χ=1.03 for all parameters except for the parameter S where χ=1.08 and the parameter E for which χ=4. The melting temperature for AISI4340 steel is taken equal to T_f=1520 °C and its conductivity k=5 W/m/°C in order to favour the adiabatic condition. The sample is impacted at a speed of 1600 mm/s, on its lower part (hollow cylinder) by a projectile made by fully thermoelastic material with the following parameters: $E = 450\ GPa$, $\nu = 0.22$, $C_v = 400\ J/Kg/°C$, $\xi = 1{,}37.10^{-5}\ °C^{-1}$ and k=50W/m/°C.

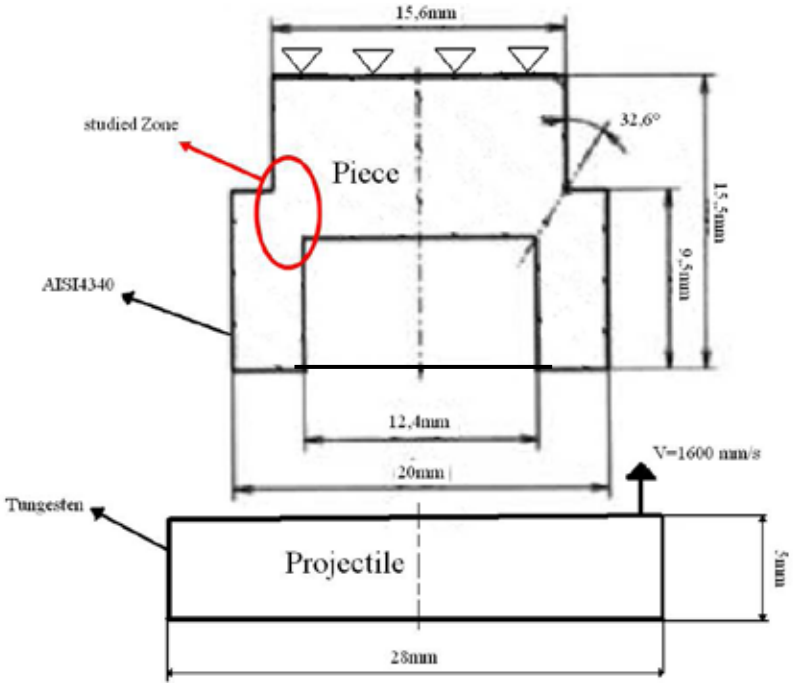

Figure 1. Schematization of the Impact test.

The geometric parameters required by the adaptive meshing procedure [26] are: $h^p_{\max}$=0.55 mm, $h^p_{\min}$=0.4 mm and $h^d_{\min}$=0.06 mm.

In this example we focus on the numerical prediction of the thermomechanical fields' localization as well as the initiation and propagation of macroscopic cracks under the impact

loading. The mesh adaptation and the distribution of the different thermomechanical fields will be investigated.

The Fig.2 shows the evolution of the mesh for different displacements of the projectile. The mesh is first refined inside the ISB where the temperature and the plastic strain are highly localized (as can bee seen in Fig 3 to 7) and mainly around the macroscopic crack where the damage has reached its maximum value. Clearly, the mesh refinement precedes the macroscopic crack path since its initiation for u = 1.95 mm (Fig. 3a) till the final fracture of the sample for u=3.26 mm (Fig. 2-c) and through the intermediate configuration as for u=2.75 mm (Fig. 2-b).

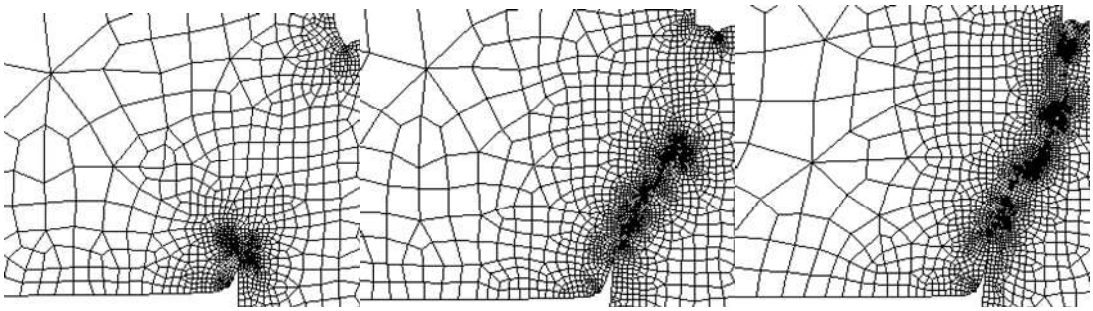

a) u=1.95 mm b) u=2.75 mm c) u=3.26 mm

Figure 2. Mesh adaptation during the macroscopic crack evolution for three different values of the projectile displacement

As shown in Fig. 3, the equivalent von Mises stress is, first, maximum with a value of 1220 MPa inside the ISB before the damage occurrence (Fig. 3a). It decreases and goes to zero as the damage increases and the macroscopic crack evolves as shown in Fig. 3a for u=1.95 mm and in Fig. 3b for u=2.75 mm. However, when the sample is completely fractured the von Mises stress is near zero every where around the crack except some zones where the contact between the crack lips generates normal stresses (Fig. 3.c). Note that this stress relaxation inside the ISB is not only due to the damage induced softening but also to the temperature increase from T_0=20 °C to T_{max}=924 °C (see Fig. 6) generated by the plastic work converted to heat.

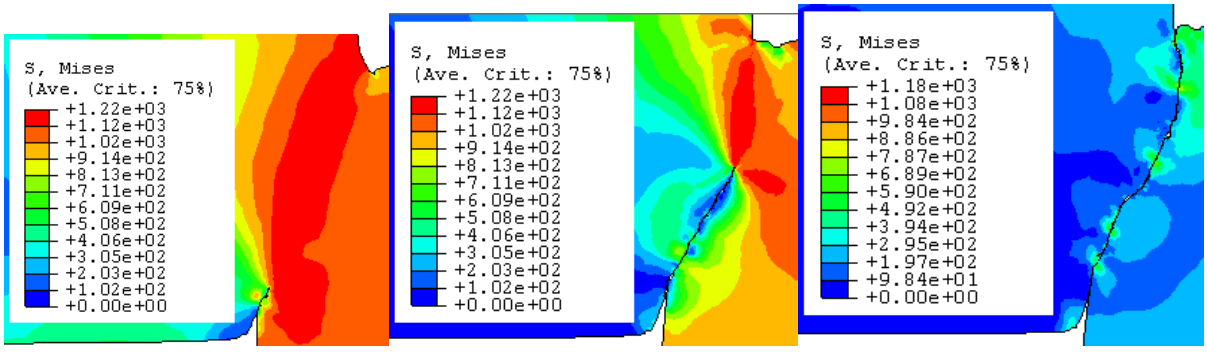

a) u=1.95 mm b) u=2.75 mm c) u=3.26 mm

Figure 3. Distribution of the von Mises equivalent stress for three different values of the projectile displacement

Similarly, the equivalent plastic strain distribution is shown in Fig.4. It is worth noting that the equivalent plastic strain localizes inside the ISB with a relatively homogeneous value around $p_{max} = 60\,\%$ every where before the macroscopic crack initiation as indicated in Fig. 4. However, once the macroscopic crack is initiated the equivalent plastic strain strongly localizes inside a very small zone located at the crack-tip where it reaches $p_{\max} = 206\,\%$ inside a small area of $p_{\max} = 155\,\%$ for u=1.95 mm as shown in Fig. 4.a. As the macroscopic crack evolves inside the ISB, the accumulated plastic strain diffuses around the crack tip and its maximum decreases to reach $p_{\max} = 137\,\%$ inside a relatively large area with $p_{\max} = 100\,\%$ for u=2.75 mm (Fig. 4b); and $p_{\max} = 132\,\%$ with a large area of $p_{\max} = 90\,\%$ for u=3.26 mm at the final fracture of the sample (Fig. 4c). This accumulated plastic strain distribution is confirmed by the equivalent plastic strain rate distribution shown in Fig. 5 where $\dot{p}_{\max} = 5.85\ 10^4\ s^{-1}$ for u=1.95 mm (Fig.5a), $\dot{p}_{\max} = 8.04\ 10^4\ s^{-1}$ for u=2.75 mm (Fig.5b) and $\dot{p}_{\max} = 3.00\ 10^5\ s^{-1}$ for u=3.26 mm (Fig.5c).

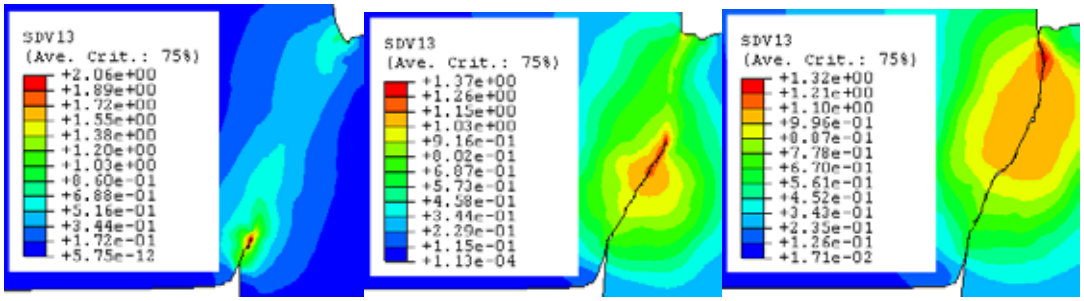

a) u=1.95 mm b) u=2.75 mm c) u=3.26 mm

Figure 4. Distribution of the equivalent plastic strain for three different values of the projectile displacement

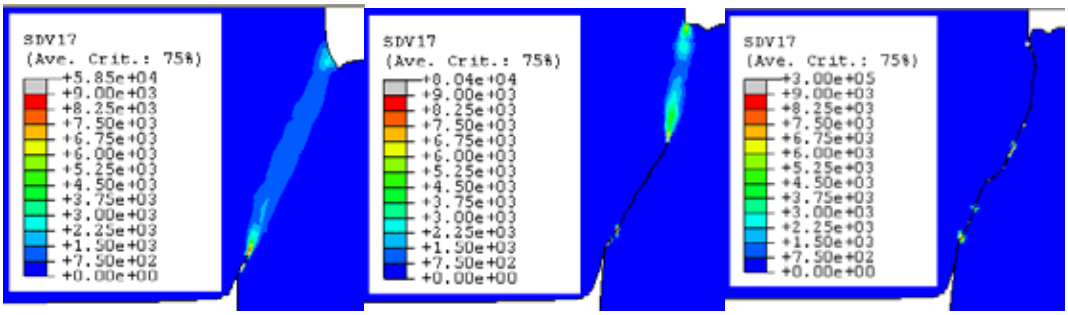

a) u=1.95 mm b) u=2.75 mm c) u=3.26 mm

Figure 5. Distribution of the equivalent plastic strain rate for three different values of the projectile displacement

The Fig.6 shows the evolution of temperature during the impact test. For the displacement u = 1.95 mm (Fig.6-a), the highest temperatures (500 ° C and 900 ° C) locate on both ends of the adiabatic shear band, for two reasons. The first is the concentration of high plastic strain rate on both ends of the band (between 3.10^3 and $9.10^3\ s^{-1}$) (Fig.6-a). The second reason is related to intense friction between the two sides of the crack which maintains high

temperatures on the edges of the crack even after the passage of the shear band (Fig.6-b) and Fig.6-c),.

The temperature localizes also inside the ISB as can be seen in Fig. 6. However, due to the friction between the crack lips, the maximum of the temperature is still located at the initial crack-initiation location with T_{max}=924 °C for u=1.95 mm (Fig. 6a), T_{max}=790 °C for u=2.75 mm (Fig. 6b) and T_{max}=817 °C for u=3.26 mm at the final fracture of the sample (Fig. 6c).

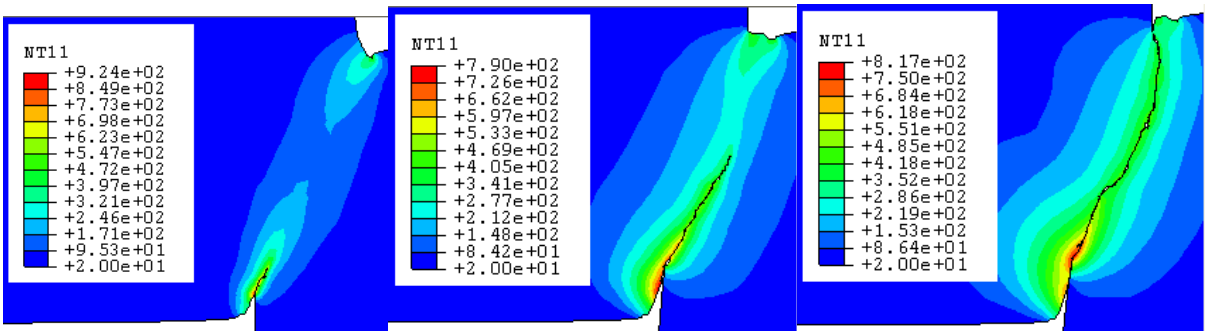

a) u=1.95 mm b) u=2.75 mm c) u=3.26 mm

Figure 6. Distribution of the temperature for three different values of the projectile displacement

Finally, the Fig.7 shows the distribution of the ductile damage including the macroscopic crack defined by killing the fully damaged elements having the smallest mesh size h_d=0.06 mm. The macroscopic crack length can be estimated to 0.5 mm for u = 1.95 mm (Fig. 7-a), 1.9 mm for u = 2.75 mm (Fig.7-b), and 3.31 mm for u = 3.26 mm (Fig. 7-c).

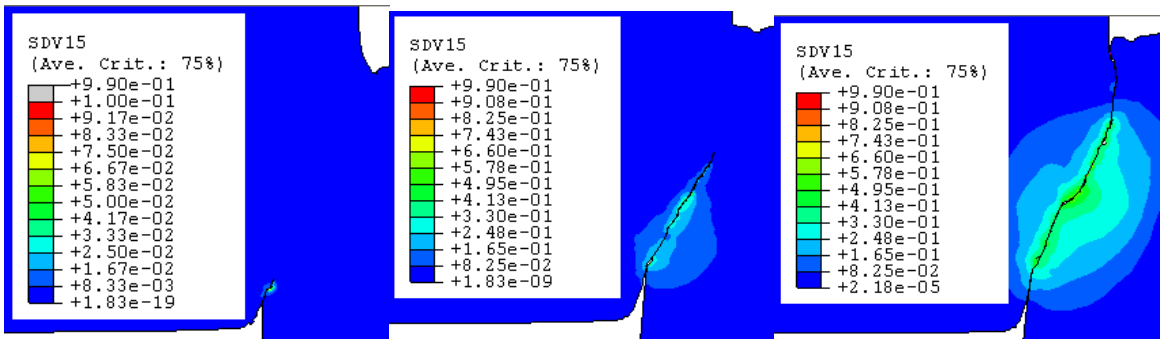

a) u=1.95 mm b) u=2.75 mm c) u=3.26 mm

Figure 7. Distribution of the ductile damage for three different values of the projectile displacement

4 CONCLUSION

An advanced thermo-elasto-viscoplastic-damage model accounting for non-linear isotropic and kinematic hardening, thermal and ductile damage effects including the micro-cracks closure under compressive phase of the loading has been briefly presented. Using the ABAQUS/EXPLICIT user's subroutine where this model has been implemented, the efficiency of this adaptive numerical methodology to simulate the dynamic fracture under high velocity impact has been shown. Particularly, this model is shown to be efficient to

capture the thermomechanical fields' localization inside an intensive shear band as well as the strong localization of the damage giving rise to the initiation and propagation of macroscopic cracks until the final fracture of the structure.

References:

[1] Taylor, G. I., " The use of flat ended projectile for determining dynamic yield stress." Par(I) Theoretical Considerations, Proc. Royal Sot Ser A194, London, 1948 pp 289-299.

[2] Lee, E. and Wolf, H., "Plastic wave propagation effects in high speed testing" J App Mech, Dec 1951 pp379-386.

[3] Ting, T. and Symonds, P, "Longitudinal Impact on Viscoplastic rods-Linear stress-strain rate law." J App Mech, June 1964 pp 199-207.

[4] Wiffens, A., "the use of flat ended projectile for determining dynamic yield stress." Par(II) Experimental Consideration, Proc. Royal Soc Ser A194, London, 1948 pp 300-322.

[5] Field JE, Walley SM, Bourne NK, Huntley JM. Experimental methods at high rates of strain. J Phys IV France 1994;4(C8):3–22.

[6] Field JE, Walley SM, Bourne NK, Huntley JM. Review of experimental techniques for high rate deformation studies. In: Proceedings of the Acoustics and Vibration Asia '98. Singapore: Acoustics and Vibration Asia 98 Conference; 1998. p. 9–38.

[7] Field JE, Proud WG, Walley SM, Goldrein HT. Review of experimental techniques for high rate deformation and shock studies. In: Nowacki WK, Klepaczko JR, editors. New experimental methods in material dynamics and impact. Warsaw, Poland: Institute of Fundamental Technological Research; 2001. p. 109–77.

[8] J.E.Field, S.M. Walley, W.G. Proud, H.T. Goldrein, C.R. Siviour, "Review of experimental techniques for high rate deformation and shock studies", International Journal of Impact Engineering 30 (2004), pp 725–775.

[9] Mackerle J., Finite-element analysis and simulation of machining: an addendum a bibliography (1996-2002), International Journal of Machine Tools and Manufacture, 2003, 43:103-114

[10] Kulak RF, Schwer LE, editors. Computational aspects of contact, impact and penetration. Lausanne: Elmepress Intl., 1991.

[11] Pantalé , O., Bacaria, J.L., Dalverny, O., Rakotomalala, R. and Caperaa, S. (2004). "2D and 3D Numerical Models of Metal Cutting with Damage Effects", Computer Methods in Applied Mechanics and Engineering, 193: 4383_4399.

[12] De Micheli, P., "Formulation explicite en tétraèdres linéaires pour la modélisation 2D et 3D de l'usinage à grande vitesse", Thèse Doctoral, Ecole nationale supérieurs des Mines de Paris. 2009.

[13] Maurel A., Fontaine M., Thibaud S., Michel G. et Gelin J.C., "Experiments and 3D FEM simulations of milling on a 304L Stainless steel, Metalforming 2008 ; Krakow.

[14] Ceretti E., Lazzaroni C., Menegardo L. et Altan T., Turning simulations using a three-dimensional FEM code, Journal of Materials Processing Technology, 2000, 98:99-103.

[15] Delalondre F., Guerdoux S., Fourment L., 3 D Simulation of Adiabatic Shear Bands in High Speed Machining, Proceeding of the 10th International Workshop on Modeling of

Machining Operations (CIRP), Reggio Calabria, 2007.
[16] Delalondre, F., "Modélisation et étude 3D des phénomènes de cisaillement adiabatiques dans les procédés de mise en forme à grande vitesse", thèse Doctorale, Ecole nationale supérieure des mines de Paris, 2008.
[17] Lin Z.C. et Yarng Y.D., A study of three-dimensional cutting model, International Journal of Computational Applications in Technology, 1996, 9(5/6):31-343.
[18] Maekawa K., Maeda M. et Tikagawa T., Simulation analysis of threedimensional continuous chip formation processes (Part1), International Japanese Society for Precision Engineering, 1997, 31(1):39-46.
[19] Molinari J.F., Three-dimensional finite-element analysis of high-speed machining, from Metal cutting and high speed machining, edited by D. Dudunski et al., Kluwer Academic/Plenum Publishers, 2002.
[20] Limido J., Espinosa C., Salaun M., Lacome J.L. "A new approach of high speed cutting modelling: SPH method", journal de physique IV, Vol. 134, 2006, pp. 1195-1200.
[21] Limido J., Espinosa C., Salaun M., Lacome J.L. "SPH method applied to high speed cutting modelling", international journal mechanical sciences, Vol. 49, 2007, pp. 898-908.
[22] Y. Chen, A. Eskandarian, M. Oskard and J.D. Lee, Meshless analysis of plasticity with application to crack growth problems, Theoretical and Applied Fracture Mechanics 41 (2004), pp. 83–94.
[23] Saanouni K., Chaboche J.L., "Computational Damage Mechanics. Application to Metal Forming", Chapter 7 of the Volume 3 : "Numerical and Computational methods" (Editors: R. de Borst, H. A. Mang), in "Comprehencive Structural Integrity", Edited by I. Milne, R.O. Ritchie and B. Karihaloo, ISBN: 0-08-043749-4, 2003.
[24] Issa M., K. Saanouni, C. Labergère, A. Rassineux, Prediction of serrated chip formation in orthogonal metal cutting by advanced adaptive 2D numerical methodology. To appear in IJMMM, 2010.
[25] Saanouni K., Lestriez P., Labergere C., « 2D adaptive FE simulations in finite thermo-elasto-viscoplasticity with ductile damage : Application to orthogonal metal cutting by chip formation and breaking »international Journal od damage Mechanics, vol 20, pp 23-61, 2011.
[26] Labergere C., Rassineux A., Saanouni K., 2D adaptive mesh methodology for the simulation of metal forming processes with damage, DOI 10.1007/s12289-010-1001-z, article in Press, 2011
[27] Rassineux A., "An automatic mesh generator for planar domains", StruCome 91, p. 519-531.
[28] Mabrouki T., Rigal J. F., "A contribution to a qualitative understanding of thermo-mechanical effects during chip formation in hard turning", J. Materials processing technology, Vol. 176, 2006.